New Approach to Designing Functional Materials for Stealth Technology: Radar Experiment with Bilayer Absorbers and Optimization of the Reflection Loss

Jaume Calvo-de la Rosa,* Aleix Bou-Comas, Joan Manel Hernàndez, Pilar Marín, Jose Maria Lopez-Villegas, Javier Tejada, and Eugene M. Chudnovsky

Microwave power absorption by a two-layer system deposited on a metallic surface is studied in the experimental setup emulating the response to a radar signal. Layers containing hexaferrite and iron powder in a dried paint of thickness under 1 mm are used. The data is analyzed within a theoretical model derived for a bilayer system from the transmission line theory. A good agreement between experimental and theoretical results is found. The advantage of using a bilayer system over a single-layer system is demonstrated. How the maximum microwave absorption (minimum reflection) can be achieved through the optimization of the filling factors and thicknesses of the two layers is shown.

1. Introduction

The absorption of microwaves by thin layers of composite materials with specially designed magnetic and dielectric properties has recently moved to the forefront of electromagnetic research by many physics, chemistry, and engineering labs, see, for example, refs. [1–3] and references therein. It has been largely driven by the military applications related to radar and stealth technology, as well as by the needs of medical, educational, and research facilities to shield rooms and equipment from the background microwave radiation that has been steadily growing in the last decades due to the increase in wireless communications.

Magnetic systems have been among the most utilized materials for that purpose[4–7] because ferromagnetic resonance naturally falls into the microwave frequency range. The research in this area has been focused on two aspects of microwave absorption. The first is related to the absorption properties of the material per se, and how effective it is in converting microwave power into heat. To provide a significant effect, the material must be dielectric. Otherwise, the absorption would be limited to the skin layer. If the material is comprised of metallic particles, they must be either coated with an insulating layer or embedded in the dielectric matrix to suppress the overall conductivity which would result in a significant reflection of the microwaves.

The second aspect of microwave absorption, which is important for applications, arises when thin layers of the absorbing material are used. It is related to the interference of microwaves reflected by the two surfaces; the most inner surface being typically interfaced with a metal. In this case, the maximum absorption by

J. Calvo-de la Rosa, J. Manel Hernàndez, J. Tejada
Departament de Física de la Matèria Condensada
Universitat de Barcelona
Martí i Franquès 1, Barcelona 08028, Spain
E-mail: jaumecalvo@ub.edu

J. Calvo-de la Rosa, J. Manel Hernàndez, J. Tejada
Institut de Nanociència i Nanotecnologia (IN2UB)
Universitat de Barcelona
Barcelona 08028, Spain

A. Bou-Comas, E. M. Chudnovsky
Graduate Program in Physics and Initiative for the Theoretical Sciences
Graduate Center
The City University of New York
New York, NY 10016, USA

P. Marín
Instituto de Magnetismo Aplicado (IMA-UCM-ADIF)
Madrid 28230, Spain

P. Marín
Departamento de Física de Materiales
Facultad de Físicas
Universidad Complutense de Madrid (UCM)
Madrid 28040, Spain

J. M. Lopez-Villegas
Departament d'Enginyeria Electrònica i Biomèdica
Universitat de Barcelona
Barcelona 08028, Spain

E. M. Chudnovsky
Department of Physics and Astronomy
Herbert H. Lehman College
The City University of New York
Bronx, NY 10468-1589, USA

**ADVANCED
SCIENCE NEWS**

www.advancedsciencenews.com

**ADVANCED
FUNCTIONAL
MATERIALS**

www.afm-journal.de

the layer should occur at the wavelength that provides destructive interference of the two reflected waves. This effect, however, has limited use because it is sharply peaked at a certain wavelength, which stealth technology and other applications of microwave absorbers cannot rely upon. To have practical importance, the absorber must be broadband, see, for example, refs.[8,9]. Our focus is on microwave absorption by magnetic bilayers. While single-layer systems have been intensively studied, with hundreds of articles entering the literature annually, experiments on bilayer systems and their theoretical analysis have been scarce.

In ref.[10], microwave absorption by nanocrystalline NiZn ferrite and iron microfibers forming single and double layers were studied in the frequency range of 2–18 GHz. The advantage of double layers in obtaining strong broadband absorption was demonstrated experimentally. A formula for the impedance (Z) of the double layer was used to fit the experimental data. Significant improvement in microwave absorption was observed. The enhancement of the absorption in the 2–18 GHz range by a double layer based upon nickel oxide and CoNiZnFeO ferrite composites, as well as the analysis of the results with the use of the impedance formula for the double layer, were reported in ref.[11]. In ref.[12], the improvement of microwave absorption properties in the 8–18 GHz range was demonstrated by using up to a 3 mm double layer of carbon black/epoxy resin and NiZn-FeO/epoxy resin. Microwave absorption by BaFeO and BaCoZn-FeO multi-nanolayers in the 7–13 GHz range was studied and analyzed with the use of the multilayer impedance formula in ref.[13]. The optimal absorption was achieved below 500 nm total thickness. The problem of thickness optimization of a double-layered microwave absorber containing magnetite particles was investigated in ref.[14]. The procedure provided a significant increase in the reflection loss in the 8–12 GHz frequency range.

Here we report our effort to optimize both aspects of microwave absorption (by the material itself and due to the destructive interference) mentioned above by experimenting with bilayers based upon magnetic particles embedded in a dielectric medium. All previously reported results were obtained by studying electric and magnetic responses to microwaves of small samples using a network analyzer, typically by means of waveguides or coaxial probes. The data were then plugged into the theoretical formula for the reflection loss by a layer and the prediction was made regarding the power absorption by a thin layer of the material. While the use of Maxwell equations for the absorbing medium is always justified, real systems always have features unaccounted for, such as fluctuations in the composition and thickness of the absorbing layer. To account for such features, we di-

rectly measure the microwave response of a thin layer or bilayer of the absorbing material deposited on a macroscopic-size metallic surface, see **Figure 1**. Such a method emulates real situations relevant to stealth and shielding technology.

The paper is structured as follows. Materials and experimental methods are described at the end of the manuscript, in Section 5. The general expression for the reflection loss by a bilayer system, which we were unable to find in textbooks or published literature, is derived in Section 2. Our experimental results and their fit by theoretical formulas are presented in Section 3. Section 4 contains a discussion of the results and suggestions for applications of microwave absorbers.

2. Bi-Layer System Absorption Model

The reflection-loss (R_L) of a single-layer material has been successfully analyzed using transmission line theory[12,13]

$$Z = Z_0 \sqrt{\frac{\mu_r}{\varepsilon_r}} \tanh\left[\left(j\frac{2\pi f d}{c} \right) \sqrt{\mu_r \varepsilon_r} \right] \quad (1)$$

$$R_L \text{ (dB)} = 20 \log \left| \frac{z/z_0 - 1}{z/z_0 + 1} \right| \quad (2)$$

where f is the frequency of the microwave, c is the velocity of light in vacuum, and d is the thickness of the material. In this section, we want to find a similar expression for a bi-layer system. In the transmission line theory, the impedance of a material can be modeled as a series of resistors, inductors, and capacitors which can be related to relative permeabilities and permitivities.[12]

Following the derivation for a single-layer impedance

$$\begin{cases} \frac{\partial v(x,t)}{\partial t} = -L(x)\frac{\partial i(x,t)}{\partial x} \\ \frac{\partial i(x,t)}{\partial t} = -C(x)\frac{\partial v(x,t)}{\partial x} \end{cases} \quad (3)$$

In a single-layer system, the capacity (C) and the induction (L) are constant. In our case, they are thickness-dependent due to the fact that there are two layers. The system of equations can be solved assuming oscillatory behavior of the magnitudes $v(x, t) = V(x)\exp(\pm j\omega t)$ and $i(x, t) = I(x)\exp(\pm j\omega t)$.

Considering a bi-layer system with the first material C_1 and L_1 and the second material of thickness d_2 characterized by C_2 and L_2 the solutions are

$$\begin{cases} V_1(x) = A\exp\left(j\omega\sqrt{L_1 C_1}x\right) + B\exp\left(-j\omega\sqrt{L_1 C_1}x\right) \\ I_1(x) = \sqrt{\frac{C_1}{L_1}}\left(-A\exp\left(j\omega\sqrt{L_1 C_1}x\right) + B\exp\left(-j\omega\sqrt{L_1 C_1}x\right)\right) \\ V(x) = E\exp\left(j\omega\sqrt{L_2 C_2}(x-d_1)\right) + F\exp\left(-j\omega\sqrt{L_2 C_2}(x-d_1)\right) \\ I_2(x) = \sqrt{\frac{C_2}{L_2}}\left(-E\exp\left(j\omega\sqrt{L_2 C_2}(x-d_1)\right) + F\exp\left(-j\omega\sqrt{L_2 C_2}(x-d_1)\right)\right) \end{cases} \quad (4)$$

**ADVANCED
SCIENCE NEWS**

www.advancedsciencenews.com

**ADVANCED
FUNCTIONAL
MATERIALS**

www.afm-journal.de

Figure 1. Schematic representation of the anechoic chamber measurement method in our experiments. GHz radiation is generated by the emitter (e) before interacting with the sample in a reflection mode and being detected by the receiver (r).

Figure 2. Experimental XRD pattern measured for HF powder sample. The most significant peaks are identified with the index of the plane corresponding to each reflection.

Imposing continuity conditions for the voltage, $V_1(d_1) = V_2(d_1)$, and for the current, $I_1(d_1) = I_2(d_1)$, yields the general expression

cause the magnetic losses (and the consequent drop in permeability) appear at a few MHz.[1] Moreover, measuring the powder

$$Z = \sqrt{\frac{L_2}{C_2}} \frac{Z_M \left(1 - \eta \tan\left(\omega\gamma_1 d_1\right) \tan\left(\omega\gamma_2\left(x - d_1\right)\right)\right) + Z_L \left(j \tan\left(\omega\gamma_1 d_1\right) + j\tan\left(\omega\gamma_2\left(x - d_1\right)\right)\right)}{Z_M \left(-\eta j \tan\left(\omega\gamma_1 d_1\right) - j\tan\left(\omega\gamma_2\left(x - d_1\right)\right)\right) + Z_L \left(\tan\left(\omega\gamma_1 d_1\right) \tan\left(\omega\gamma_2\left(x - d_1\right)\right) - \eta\right)} \tag{5}$$

where $\eta = \sqrt{C_1 L_2 / L_1 C_2}$ and $\gamma_i = \sqrt{C_i L_i}$. The quantities Z_M and Z_L are the impedances of the material and the transmission line respectively and $x > d_1$.

The material impedance is set to zero. In $\gamma_i = \frac{\sqrt{\epsilon_i \mu_i}}{c}$, where we have dropped the subindex r, ϵ_i and μ_i are relative permeability and permittivity respectively, and $\sqrt{L_i / C_i} = \sqrt{\mu_i / \epsilon_i} Z_0$. We obtain the following expression (that reduces to the single layer impedance if the same material for both layers is considered)

$$Z = -Z_0 \frac{\sqrt{\frac{\mu_1}{\epsilon_1}} \tanh\left(j \frac{2\pi\omega}{c} \sqrt{\epsilon_1 \mu_1} d_1\right) + \sqrt{\frac{\mu_2}{\epsilon_2}} \tanh\left(j \frac{2\pi\omega}{c} \sqrt{\epsilon_2 \mu_2} d_2\right)}{1 + \sqrt{\frac{\mu_1 \epsilon_2}{\epsilon_1 \mu_2}} \tanh\left(j \frac{2\pi\omega}{c} \sqrt{\epsilon_1 \mu_1} d_1\right) \tanh\left(j \frac{2\pi\omega}{c} \sqrt{\epsilon_2 \mu_2} d_2\right)} \tag{6}$$

3. Results

The synthesized barium hexaferrites (HF) were first chemically and crystallographically characterized by X-ray diffraction (XRD). **Figure 2** shows the diffraction patterns obtained for each sample. The analysis of these patterns confirms the expected composition. No impurities or further structures were detected.

The HF and Fe powder samples, together with the commercial paint, were all electromagnetically characterized in the GHz frequency range with the coaxial probe. The Nicolson–Ross–Weir (NRW) model[12–14] was used to deduce the complex magnetic permeability and dielectric permittivity from the measured complex S-parameters. In the case of the paint, which is a non-magnetic material, the NRW method has been adapted to pure dielectric conditions.[15] **Figure 3** depicts the complex spectra obtained for each of the three materials, both for the electric and magnetic contributions.

As it may be observed, the Fe permeability (Figure 3E) is lower than the typical one at the kHz and MHz frequency range be-
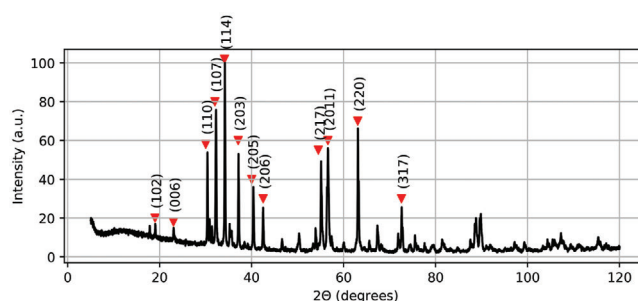
samples instead of bulk ones may increase the demagnetization field effects, which leads to a decrease in the measured permittivity as well. Nonetheless, this is still the component that provides the highest magnetic permeability in the system. Besides, the metallic particles' permittivity is also large (Figure 3D) given that their free electrons may easily be displaced by the electric field, leading to a strong polarization.

The effective electromagnetic properties of the sheets (which contain a mixture of paint and functional powder) have been modeled by using the Maxwell–Garnett (MG) model[16,17]

$$\frac{\epsilon_{\text{eff}} - \epsilon_h}{\epsilon_{\text{eff}} + 2\epsilon_h} = ff_v \frac{\epsilon_i - \epsilon_h}{\epsilon_i + 2\epsilon_h} \tag{7}$$

where ϵ_{eff} refers to the effective (paint + powder) permittivity, while ϵ_h and ϵ_i refer to the host (paint) and inclusions (powder) permittivity. The same conversion has been done with the permeability. Given that this model depends on the volume filling factor (ff_V), reference densities of 1.50, 5.30, and 7.87 gcm^{-3} have been used for the paint, ceramic, and metallic components, respectively, for converting the weight fill factor (ff_W) to the volumetric one (ff_V). The resulting effective electromagnetic properties are, obviously, dependent on the filling factor. Given that our sheets are not uniform and therefore we do have a concentration gradient in the radial direction, we have run this computation for different ff_V (i.e., ff_W) to produce a clear picture of the electromagnetic properties of the samples. This modeling is represented in **Figure 4**, which shows the complex permittivity and permeability obtained for each mixture of materials and ff_W of 4%, 20%, 40%, 60%, and 80%, which correspond to ff_V of 1.17%, 6.61%, 15.87%, 29.80%, and 53.01% for samples containing HF (P1, P2, and P3), and ff_V of 0.79%, 4.55%, 11.27%, 22.23%, and 43.26% for those with Fe powder (P4, P5, and P6).
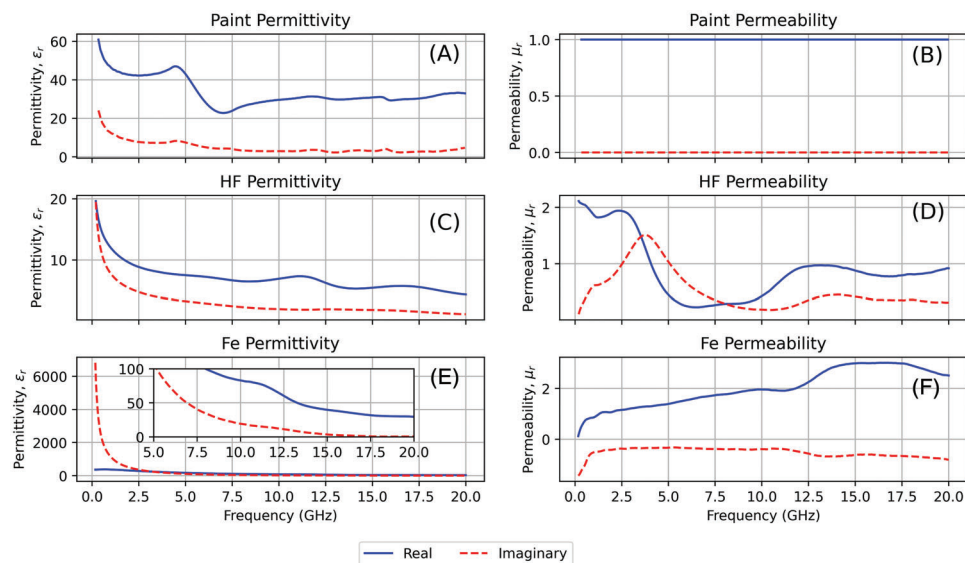
**ADVANCED
SCIENCE NEWS**

www.advancedsciencenews.com

**ADVANCED
FUNCTIONAL
MATERIALS**

www.afm-journal.de

Figure 3. Complex permittivity (left column) and permeability (right column) for the paint (A,B), the hexaferrite (C,D), and the iron powder (E,F). Data obtained after processing the *S*-parameter through the NWR method.

As it may be observed, for low filling factors, both components have very similar electromagnetic properties compared to pure paint, which is the major component. While the filling factor increases, the effective properties tend to be closer to the ones of the functional particles dispersed in the paint and each type of layer starts to have a more particular behavior. As it has been mentioned before, our sheets have a global $ff_w = 4\%$ but have a concentration gradient from the center to the edges. Therefore, at the center of the sheet $ff_w > 4\%$, where the interaction with the electromagnetic radiation is stronger. According to our esti-

mations, the sheets have $ff_w \approx 11\%$ at the 15×15 cm^2 central region, $ff_w \approx 25\%$ at the central 10×10 cm^2, or even $ff_w \approx 70\%$ at the 6×6 cm^2 central part. Therefore, we must consider later with our model the possibility of having these considerable amounts of loading at the region with the strongest electromagnetic interaction.

With these permittivity and permeability complex data, we first validate the R_L results obtained for each individual layer. To do so, we compare the experimentally measured R_L at the anechoic chamber with the R_L calculated by the transmission line theory
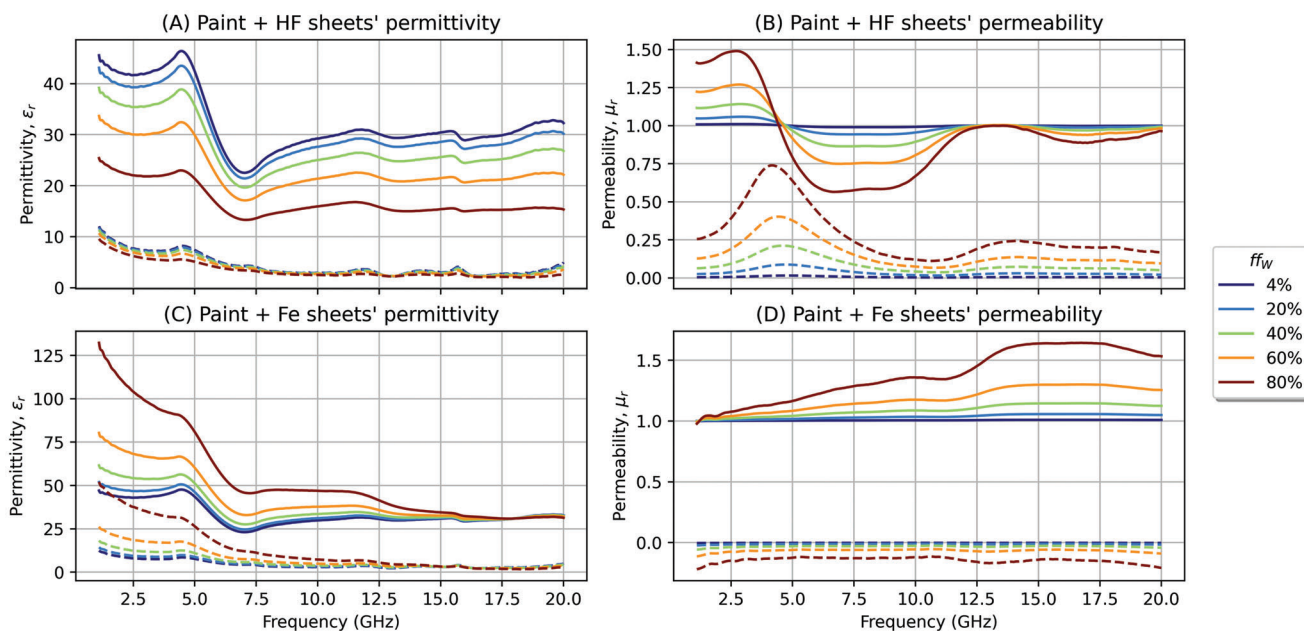

Figure 4. Modeling of the mixture's effective properties by applying the MG model to the permittivity and permeability data of each of the components using ff_w of 4%, 20%, 40%, 60%, and 80%. Solid lines represent the real part, while dashed lines refer to the imaginary one.
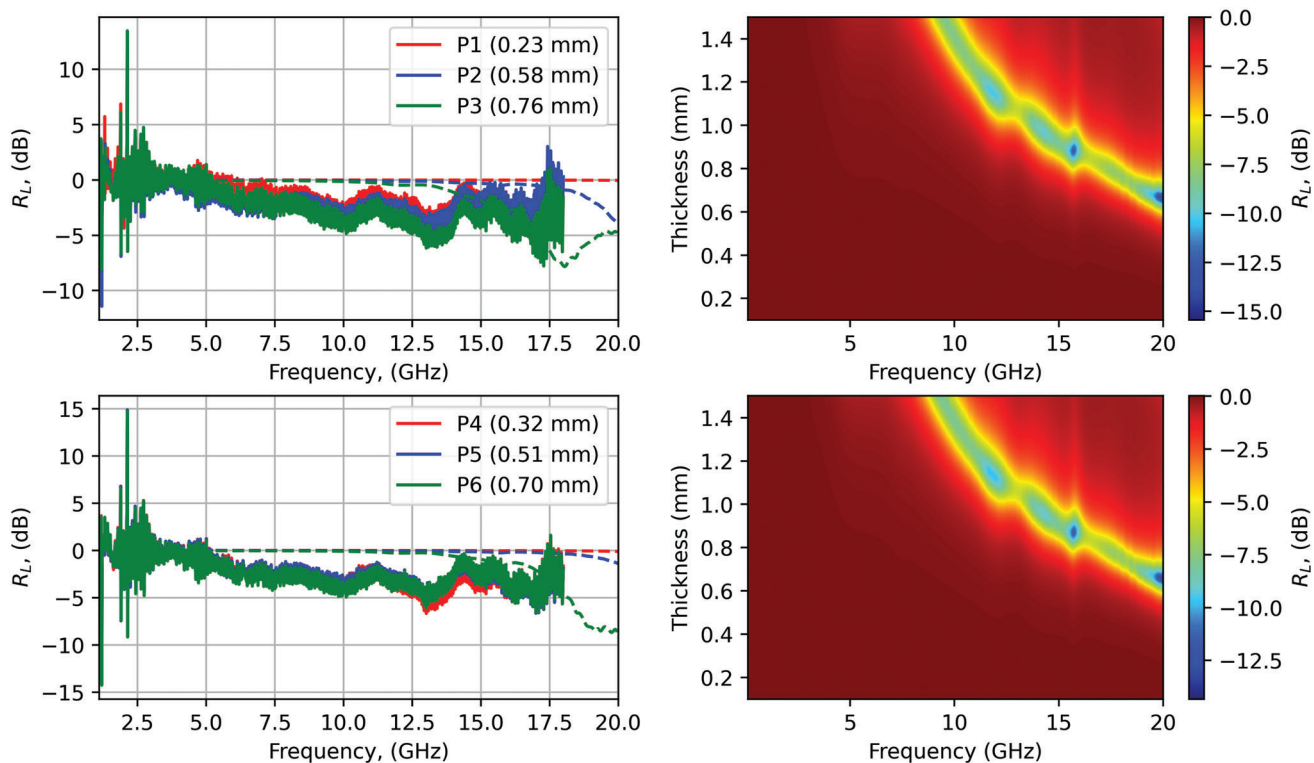
**ADVANCED
SCIENCE NEWS**

www.advancedsciencenews.com

**ADVANCED
FUNCTIONAL
MATERIALS**

www.afm-journal.de

Figure 5. Comparison between the experimental and calculated data for the sheets containing ff_W = 4% of *HF* (top row) and Fe (bottom row) particles. Left side plots correspond to the comparison for the specific thicknesses prepared at the laboratory, while on the right side, there is a 2D simulation of the expected R_L for sheets between 0.1 and 1.5 mm. Solid lines correspond to experimental data, while dashed lines correspond to the calculated values.

using the sheets' electromagnetic properties measured before. This comparison is represented in **Figure 5**, being the first row of subplots devoted to sheets P1–P3 (paint + HF) and the second one to P4–P6 (paint + Fe). In each case, first, the comparison between the experimental and calculated values is done for the three thicknesses prepared at the laboratory. On the right side, a 2D R_L simulation for a wider and continuous range of thicknesses is done in order to have a broad view of the expected absorption of each sheet, even outside of the experimental domain. The agreement between the experimental and the calculated R_L data has been verified from ff_w = 4% to 80%.

One may immediately see that none of the layers presents significant electromagnetic absorption when being irradiated with microwaves between 0.5 and 18 GHz. The spectra are flat and the small deviation from the zero is attributed to experimental noise. The calculations done with the single-layer transmission line theory reinforce these observations, as no absorption is expected in this frequency range for any of the compositions used.

The 2D simulations provide some additional information of interest. According to these predictions, we should not observe any absorption peaks for samples thinner than 0.8 mm below 18 GHz, as happened in the real radar experiments. Moreover, these results suggest that slightly thicker samples would start to absorb radiation in this frequency range. This prediction agrees with the experimental data, which seems to show the start of a peak at the top frequency limit for the thicker sample, for both types of samples. These simulations also predict that absorptions up to 12.5 and 15 dB would be feasible for the HF and Fe

sheets, respectively. Given that both types of sheets have a predominant paint content (and thus, their electromagnetic properties do not diverge that much) the resultant R_L spectra are also similar, though small changes are appreciated due to the functional powder effect.

Once single-layer systems have been discussed, we move to double-layer systems, which represent a much more unexplored territory in literature, both theoretically and experimentally. To do so, again we provide a detailed comparison between the anechoic chamber measured data and the predictions done by our own model using the measured complex electromagnetic properties. Let us start by analyzing a system consisting of the combination of the thickest HF layer (P3) with the different thickness Fe sheets, that is, we have a system of two layers with different electromagnetic properties and varying thickness. **Figure 6** below shows the experimental data, measured in the anechoic chamber, together with the calculation from the bilayer model for ff_w = 20%, 40%, 60%, and 80%.

As a first observation, it must be highlighted that the model is capable, in all cases, to reproduce with reasonable accuracy the peak position, amplitude, and shape from the thickness and complex permittivity and permeability data. Looking in more detail, we may observe that—as is expected from the gradient in particles' concentration—the agreement is not so good for low-filling factors. However, when the filling factor is increased, the theoretical and the experimental data match. The best agreement is reached for ff_w = 60%, giving us an idea about the real filling factor at the center of the sheet. If the ff_w becomes too high (80%), the
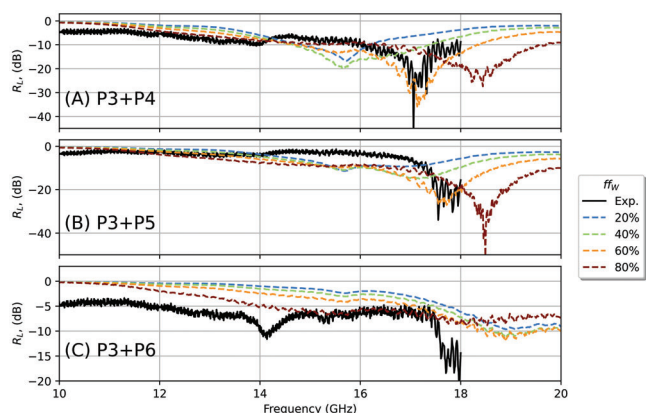
**ADVANCED
SCIENCE NEWS**

www.advancedsciencenews.com

**ADVANCED
FUNCTIONAL
MATERIALS**

www.afm-journal.de

Figure 6. Comparison between the experimental (solid black) R_L measured in the anechoic chamber and the R_L data calculated by the model (dashed) with ff_w = 20%, 40%, 60%, and 80%, for the bilayered systems A) P3+ P4, B) P3+P5, and C) P3+P6.

agreement deteriorates. For cases (A) P3+P4 and (B) P3+P5 the agreement is quite extraordinary, while in (C) P3+P6 the model tends to predict the peak that seems to move to the frequency range above 18 GHz.

From Figure 6A, it is possible to extract a few interesting conclusions. As one may observe, if the filling factor is too high (80%) the agreement worsens and the amplitude of the calculated peak is reduced. This highlights the importance of optimizing and selecting the appropriate filling factor in the material design process and during the computational simulation of R_L. In the first case, this is a crucial aspect, just increasing the magnetic powder load does not always result in the increase of the power absorption. It is necessary to optimize the filling factors based on the electromagnetic properties of each component, to reach the adequate effective permittivity and permeability that create an impedance match between the two layers of specific thickness. That is a crucial point because, from the modeling perspective, the reflection loss has a *tanh* dependence on the permittivity, permeability, and thicknesses of the two layers, so it is very sensitive to small changes in these variables. Such an optimization within our theoretical model is shown in **Figure 7**.

The simulations shown in the figure above are a powerful tool for design processes of high absorption materials. In the first case, Figure 7A represents the average reflection loss produced by the sample all along the analyzed frequency range. Therefore, it is affected by the peak base but not only by the maximum peak amplitude, leading to logic smaller R_L. Nonetheless, this figure is of great importance because it shows the overall absorption behavior of the material along the frequency range, considering both the peak amplitude and width. On the other hand, Figure 7B represents the maximum absorption (minimum R_L) achieved for each combination of thicknesses between the two layers. As it may be observed, losses around 40–50 dBs may be easily achieved with a first layer of thickness between 0.5 and 1 mm and below 0.5 mm in the second one. As stated before, the constant increase in thickness does not lead to a permanent increase in absorbed power. Thus, optimizing the relative thickness between layers is a crucial factor do design materials with the best possible shielding capabilities. Finally, Figure 7C provides a clear view of the de-
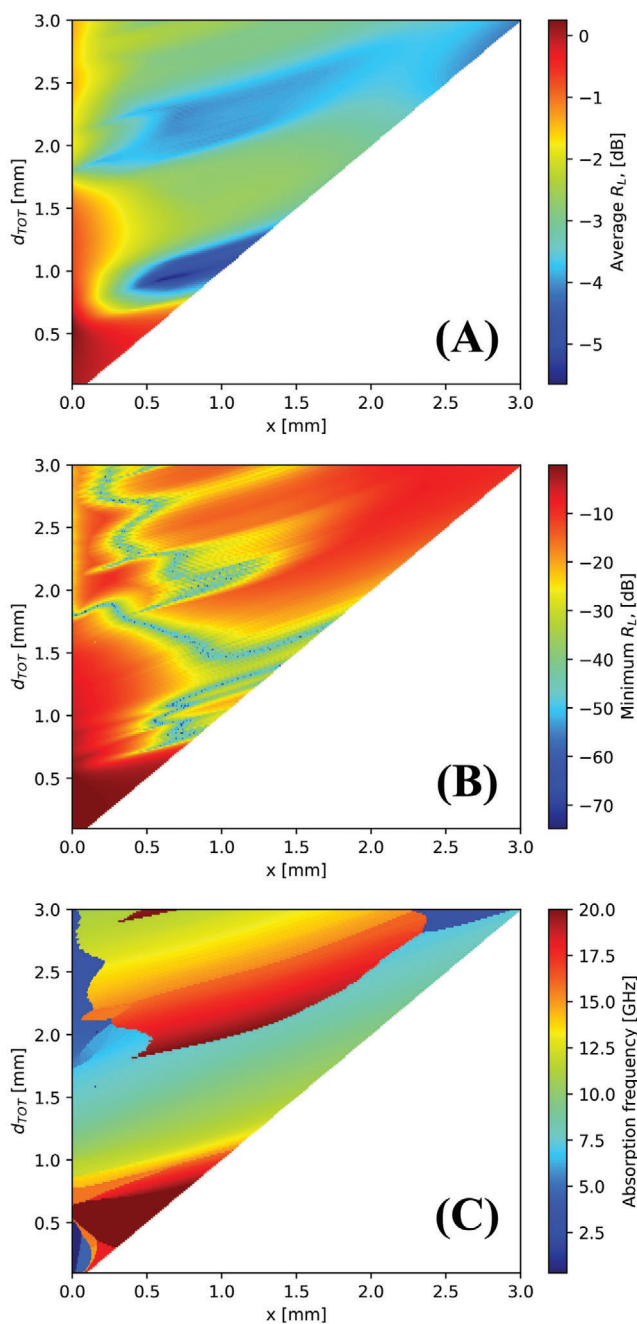

Figure 7. 2D simulation of the A) average R_L, B) minimum R_L (maximum absorption), and C) absorption frequency as a function of the thickness of each layer in a bi-layer system. x refers to the thickness of the first layer, while d_{TOT} is the total thickness of the bilayer.

pendence of the resonance (and thus, absorption) frequency on the thicknesses of the two layers. One may find discontinuities in this spectrum (i.e., abrupt changes in frequency), which may either be due to the noise contribution when the peak's signal-to-noise ratio is low or because in some cases there may be several absorption peaks with one stronger than the others.

**ADVANCED
SCIENCE NEWS**

www.advancedsciencenews.com

**ADVANCED
FUNCTIONAL
MATERIALS**

www.afm-journal.de

4. Conclusion

We have studied microwave absorption by a two-layer system containing powders of iron and barium hexaferrite particles. Layers under 1 mm thickness of dried paint containing the particles were deposited on a metallic surface. The reflection loss has been studied in an experiment emulating response to a radar signal. This differs from the experiments reported in the literature, where the reflection loss was not directly measured but calculated from the data on the frequency dependence of real and imaginary parts of permittivity and permeability. While such experiments are valuable, they ignore many features present in the reflection of a radar signal such as the geometry of the reflecting system and inhomogeneity of the parameters.

We began by establishing that the material of paint, which dominated the composition of the layers, was not responsible for any reflection loss. We then studied microwave absorption by single layers of different thicknesses and filling factors. The measured reflection loss from single layers was compared with a theoretical formula and a good agreement was found. The magnitude of the reflection loss for single layers was low, however, at frequencies up to 18 GHz in all ranges of the parameters used. The observed absorption changes substantially with any changes in the effective permittivity or permeability of any of the two layers. This occurs by either changing the functional filler powders or by changing the filling factor. Any change in the electromagnetic properties of the layers requires a new optimization of their thicknesses to maximize the absorption.

This changed dramatically when we moved to a bilayer system with the same parameter ranges for single layers. The reflection loss in some cases has grown tenfold, while still allowing the total thickness of the bilayer system under 1 mm. The data were analyzed with the use of a theoretical expression for a bilayer system derived by methods of the transmission line theory. A good agreement between experimental and theoretical results has been found. The ratio of the thicknesses of the two layers as an additional optimization parameter in the impedance match has been shown to play a pivotal role in the enhancement of the reflection loss.

5. Experimental Section

The preparation of the absorbing samples required multiple components that needed to be carefully processed in order to produce sheets with the desired properties. The most significant element in this preparation was the functional powder, which was the material that provided the specific dielectric and magnetic character to the sample. Two types of powder materials were worked with: barium-hexaferrite ceramic materials (noted as "HF") and soft magnetic iron particles (referred to as "Fe"). The Fe powders were provided by AMES enterprise and a complete structural and magnetic characterization may be found in the previous works.[1,2] It consisted of Fe-core particles of 100 µm in diameter with high permeability, which were widely used for kHz and MHz applications. The core's crystallinity was high, and no impurities were detected by XRD. On the other hand, the HF powder samples were synthesized by own at the laboratory and were selected for this work because they have an extended reputation as microwave absorbers.[8–11]

Synthesis of Functional Powder: The barium hexaferrite ($BaFe_{12}O_{19}$) powder was synthesized through a conventional co-precipitation route. Stoichiometric amounts of $Ba(NO_3)_2$ and $Fe(NO_3)_3 \cdot 9H_2O$ (Scharlab, as

Table 1. Description of the prepared sheets.

Sheet ID	Contained powder ID	Total thickness [mm]
P1	HF	0.23 ± 0.07
P2	HF	0.58 ± 0.05
P3	HF	0.76 ± 0.09
P4	Fe	0.32 ± 0.09
P5	Fe	0.51 ± 0.08
P6	Fe	0.70 ± 0.06

Thickness values are obtained as the average of four measurements at the sheet's contour.

received) were dissolved in 300 mL of deionized water under continuous stirring at room temperature for 2 h. Once complete dissolution was reached, a 2 M solution of NaOH was added dropwise until it reached pH ≈ 10. The brown precipitate was cleaned and separated from water by doing three cycles of 10 min of centrifugation at 3000 rpm with ethanol. The obtained solid part was dried for 24 h at 80 °C and then ground to powder with a mortar before being heated at 900 °C for 2 h in a furnace. The final product was finally grounded again.

Sheets Preparation: The functional powders needed to be later processed in order to produce 2D sheets, in such a way that the material could be deposited into a surface. To do so, the functional powder was mixed with paint (commercial Titan's Unilak white water enamel) in a 4–96% weight fraction (f_W), respectively. The mixture was then manually deposited on top of a 50 µm thickness polyester sheet of 25 cm × 25 cm. The painted sheets were left to dry at room temperature for 24 h.

For each type of functional powder, three different sheets varying the total thickness were prepared, as described in **Table 1** below. Therefore, it was not only able to evaluate the effect of the intrinsic electromagnetic properties of the powder dispersed on it but also to figure out the repercussions that a geometrical aspect had on the absorption procedure.

Due to the manual deposition method used for the sheets' preparation and the elevated density of the magnetic powder, the obtained sheets did not show a homogeneous dispersion of magnetic particles along their surface. Consequently, all sheets showed a larger concentration of particles at their central region compared to the perimeter, leading to an effective gradient of filling factor from the center to the borders.

Characterization: Powder XRD measurements were done by using a PANalytical X'Pert PRO MPD θ/θ Bragg–Brentano powder diffractometer of 240 mm radius using Cu *K*-alpha radiation (λ = 1.5418 Å). The static magnetic properties from powder samples were measured through a Quantum Design MPMS SUperconducting QUantum Interference Device (SQUID) magnetometer. On the other hand, in order to measure the complex magnetic permeability and dielectric permittivity in the microwave region (from 0.05 to 20 GHz), a coaxial probe was designed by using two coaxial 3.5 mm connectors coupled to a Keysight E5071C ENA Series Network Analyzer. The system was electronically calibrated prior to the measurements and two-port *S* parameters were recorded along 1601 points from 0.05 to 20 GHz. Port-extension correction was also done to all the measurements to deal with all the potential signal phase shifts due to the probe dimensions. Finally, the experimental absorption of the sheets was measured inside an anechoic chamber. The sample was subjected to a metallic plate while two antennas were oriented in reflection configuration (see Figure 1). An Agilent E8362B PNA Series Network Analyzer was connected to the antennas and the reflection loss was recorded along 1601 points from 0.5 to 18 GHz.

Acknowledgements

Conflict of Interest

The authors declare no conflict of interest.

Data Availability Statement

The data that support the findings of this study are available from the corresponding author upon reasonable request.

Keywords

[1] J. Calvo-De La Rosa, J. Tejada, A. Lousa, *J. Magn. Magn. Mater.* **2019**, *475*, 570.

[2] J. Calvo de la Rosa, Universitat de Barcelona, https://diposit.ub.edu/dspace/handle/2445/144801 (accessed: March 2023).

[3] E. M. Chudnovsky, D. A. Garanin, *Phys. Rev. B* **2023**, *107*, 224413.

[4] H. Ahmad, A. Tariq, A. Shehzad, M. S. Faheem, M. Shafiq, I. A. Rashid, A. Afzal, A. Munir, M. T. Riaz, H. T. Haider, A. Afzal, M. B. Qadir, Z. Khaliq, *Polym. Compos.* **2019**, *40*, 4457.

[5] X. Zeng, X. Cheng, R. Yu, G. D. Stucky, *Carbon N Y* **2020**, *168*, 606.

[6] H. Pang, Y. Duan, L. Huang, L. Song, J. Liu, T. Zhang, X. Yang, J. Liu, X. Ma, J. Di, X. Liu, *Composites, Part B* **2021**, *224*, 109173.

[7] P. Sahoo, L. Saini, A. Dixit, *Oxford Open Mater. Sci.* **2023**, *3*, itac012.

[8] A. Houbi, Z. A. Aldashevich, Y. Atassi, Z. Bagasharova Telmanovna, M. Saule, K. Kubanych, *J. Magn. Magn. Mater.* **2021**, *529*, 167839.

[9] M. Rani, K. S. Bhatia, H. Singh, H. Kaur, N. Gupta, *SN Appl. Sci.* **2020**, *2*, 2035.

[10] S. V. Trukhanov, A. V. Trukhanov, V. G. Kostishyn, L. V. Panina, A. V. Trukhanov, V. A. Turchenko, D. I. Tishkevich, E. L. Trukhanova, O. S. Yakovenko, L. Y. Matzui, *Dalton Trans.* **2017**, *46*, 9010

[11] G. Gultom, M. Rianna, P. Sebayang, M. Ginting, *Case Stud. Therm. Eng.* **2020**, *18*, 100580.

[12] F. Costa, M. Borgese, M. Degiorgi, A. Monorchio, *Electronics* **2017**, *6*, 95.

[13] A. M. Nicolson, G. F. Ross, *IEEE Trans. Instrum. Meas.* **1970**, *19*, 377.

[14] R. A. Speciale, *IEEE Trans Microwave Theory Tech* **1977**, *25*, 1100.

[15] C. Tsipogiannis, *Master Thesis*, Lund University, Sweden;https://lup.lub.lu.se/luur/download?func=downloadFile%26recordOId=3359623%26fileOId=3359627.

[16] J. C. Maxwell Garnett, *Philos. Trans. R. Soc. London, Ser. A* **1904**, *203*, 385.

[17] A. Sihvola, *Subsurf. Sens. Technol. Appl.* **2000**, *1*, 393.